Mathematical Modelling in Civil Engineering
Vol. 20-No. 1: 42-56-2025
10.2478/mmce-2025-0004

ESTIMATION OF NONLINEAR SEISMIC RESPONSE OF A 10-STORY RC SHEAR WALL STRUCTURE DESIGNED ACCORDING TO P100/81

Mihai PLATON – Assistant, PhD Student, Technical University of Civil Engineering, Faculty of Civil Engineering, Bucharest, Romania, e-mail: (mihai.platon@phd.utcb.ro)

Abstract: This study analyzes the displacement demands of a 10-story reinforced concrete (RC) building with shear walls, designed according to the P100/81 seismic code. The nonlinear static (pushover) analysis evaluates the structure's seismic performance, identifying dynamic characteristics, plastic mechanisms, and displacement demands for key limit states: Immediate Occupancy, Life Safety, and Collapse Prevention. Displacement demands are determined by intersecting pushover curves with inelastic spectra, using either Miranda's method or artificially generated spectra for various mean return intervals (MRI). The results emphasize the importance of displacement demand evaluation to identify vulnerable structural elements and the necessity of retrofitting measures to improve seismic resilience and ensure compliance with modern standards.

Keywords: Nonlinear Seismic Response, Reinforced Concrete Shear Walls, PUSH-OVER Analysis, Displacement Demand.

1. Introduction

The seismic behavior of reinforced concrete (RC) structures remains a critical area of study in structural engineering, particularly in regions prone to seismic activity. This paper focuses on analyzing the nonlinear seismic response of a 10-story building with RC shear walls, designed in compliance with the seismic code P100/81 [1]. The study provides insights into the dynamic characteristics of the structure, emphasizing the significance of pushover analysis as a tool to assess the building's performance under lateral seismic forces.

The research employs modern computational techniques to evaluate the building's capacity to withstand seismic loads while adhering to the design principles established in P100/81. By exploring the relationship between structural design and seismic response, the article contributes to the understanding of the inherent vulnerabilities and strengths of RC shear wall structures in the context of older seismic design standards. The findings aim to inform both structural retrofit strategies and the development of improved seismic codes for future applications.

The building depicted (M2 tr.A) in the attached plans (Fig. 1 & Fig. 2) is part of a complex consisting of three sections, constructed around 1983. Located in the Pantelimon neighborhood of Bucharest, the complex showcases the layout and internal functionalities of the residential block.

Specifically, the complex comprises 11 above-ground levels, featuring various mixed-use spaces on the ground floor.

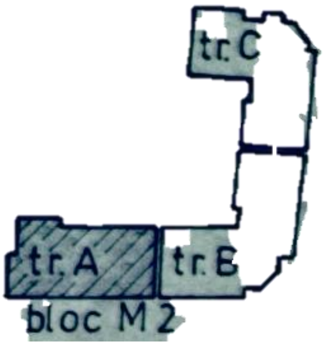

Fig. 1 - Ensemble of Sections (Original Execution Plans)

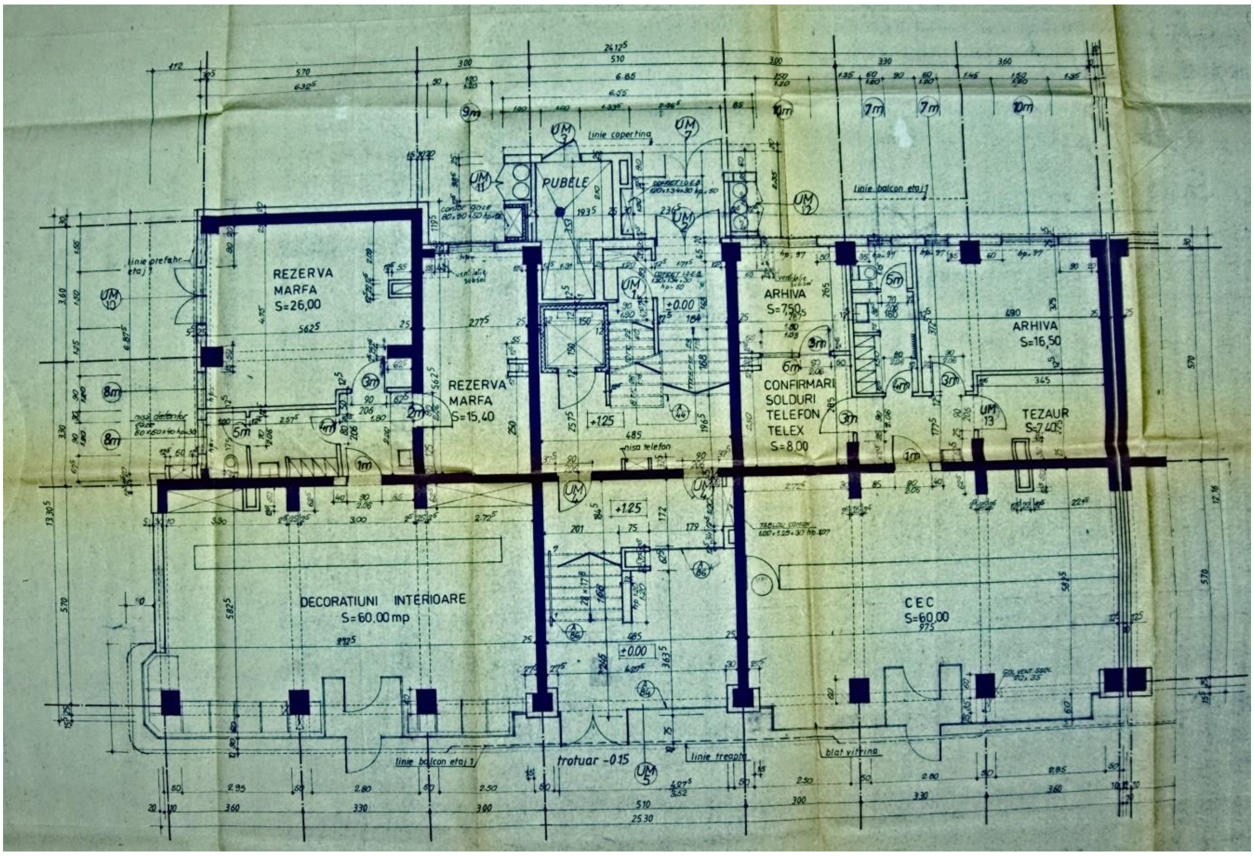

Fig. 2 - Ground Floor Plan (Original Execution Plans)

2. Structural System

2.1 Description of the Load-Bearing Structure

The building in question has 12 levels: basement, ground floor, 10 stories, and a technical floor. The basement spans the entire footprint of the structure, with variable heights ranging from 1.85 to 3.25 meters. It is enclosed by reinforced concrete perimeter walls with a thickness of 30 cm. The internal compartmentalization of the basement is also achieved through 30 cm thick reinforced concrete walls, contributing to the "rigid box" concept implemented to maximize the seismic resistance of the structure. It is worth noting that these walls are distributed along every axis of the structure, with door openings provided to ensure access to the storage rooms located in the basement.

The slab above the basement is monolithic, with a thickness of 15 cm. The foundations consist of continuous beams with footing thicknesses generally measuring 2.00 meters, positioned beneath each concrete wall.

The superstructure of the building incorporates orthogonally arranged walls in both directions, with thicknesses of 25 cm. Beams are placed both along the building’s perimeter and within certain rooms. The slabs above each floor are made of reinforced concrete with a thickness of 13 cm, consisting of 5 cm prefabricated panels topped with an 8 cm concrete overlay. This technical solution was adopted to enhance thermal and acoustic performance while also facilitating the construction pace.

The columns of the building, with a constant cross-section of 50 x 60 cm throughout the height, are designed to ensure vertical rigidity, primarily serving to bear gravitational loads.

2.2 Material Used

The B300 concrete used in this construction was reclassified to C18/22.5 under current standards (EN 1992-1-1/2004 [2]), with an estimated modulus of elasticity of 29.3 GPa. Regarding the reinforcement, reinforced steel PC60, PC52, and OB37 were used.

2.3 Vertical Mass Distribution

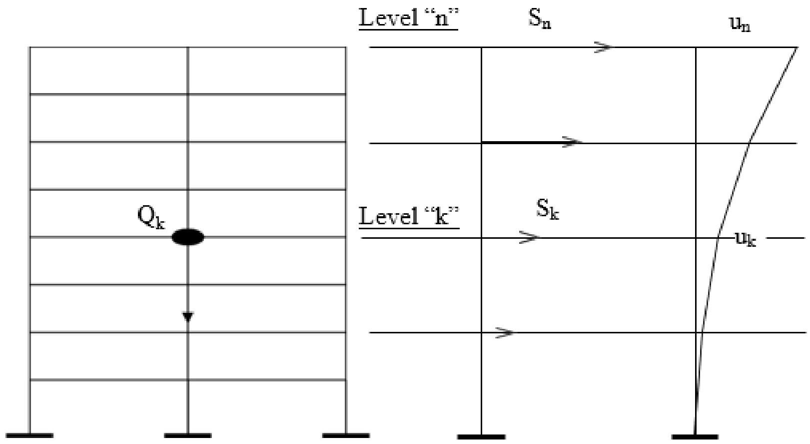

Fig. 3 - Vertical Mass Distribution

Table 1

Story masses and their distribution

Level	Qk [kN]	uk
Story 1	4543.5512	0.1261
Story 2	3904.7213	0.2135
Story 3	3904.7213	0.3009
Story 4	3904.7213	0.3883
Story 5	3904.7213	0.4756
Story 6	3904.7213	0.563
Story 7	3904.7213	0.65
Story 8	3904.7213	0.7378
Story 9	3904.7213	0.8252
Story 10	4676.8897	0.9621
Story 11	4233.277	1

2.4 Short description of columns and walls

Columns: Columns have a rectangular 50×60 cm cross-section with 4 reinforcement bars on the short side and 5 on the long side.

Longitudinal reinforcement: At the ground floor and first floor, Type S1 columns use 12 bars of 16 mm, while Type S1′ columns use 8 bars of 16 mm and 6 bars of 14 mm. At higher floors, smaller diameter bars are used with additional reinforcement detailing at the corners and along the sides. All reinforcement is made from PC60 steel.

Stirrups: 8 mm diameter, four-legged stirrups made from PC52 steel secure the longitudinal bars. They are spaced at 10 cm in the upper and lower thirds (critical zones) and 20 cm elsewhere to enhance seismic resistance and prevent buckling.

Walls: Walls maintain a constant thickness of 25 cm throughout the structure.

Transverse Reinforcement: At each wall end, PC52 steel transverse bars confine the concrete and prevent the buckling of longitudinal bars, enhancing seismic resistance.

Longitudinal Reinforcement: Walls use PC60 longitudinal bars anchored over 45 diameters for even stress distribution. On the ground and first floors, 8 mm bars are typically spaced at 20 cm (with some areas using 12 mm), while higher levels use 8 mm bars at 25 cm spacing or 10 mm bars at 20 cm spacing—with welded 5 mm wire mesh added on the top story.

The wall end zones ("bulbs") are reinforced with bars ranging from 12 mm to 25 mm, secured with stirrups (8 mm or 6 mm) spaced at 12 cm on the ground floor and 15 cm on upper levels.

3. Determination of the modal characteristics of the building

3.1 Structural Assumptions

It is assumed that the structure is fixed at its base, an idea justified by the presence of a basement enclosed by perimeter and partition reinforced concrete walls with thicknesses of 25 cm and 30 cm. The additional stiffness provided by the 15 cm-thick slabs over the basement, together with the basement walls, indicates a significant rigidity difference between the ground floor and the basement, allowing the basement to be treated as an “infinitely rigid box”. In the analysis, a 5% fraction of critical damping was taken.

3.2 Stiffness of Structural Elements

Columns and Beams (Bending Stiffness): Taken as 0.50 of the gross EI (product of the elastic modulus and the moment of inertia).

Slabs (Axial Stiffness): Taken as 0.70 of the uncracked, gross section.

Walls (Bending Stiffness): Taken as 50% of the value corresponding to the uncracked, gross section.

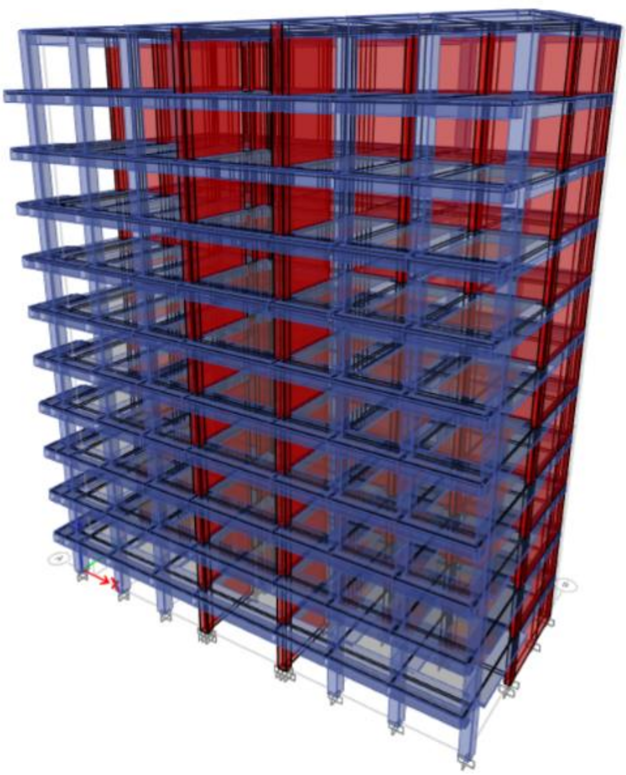

Fig. 4 - 3D Computational Model

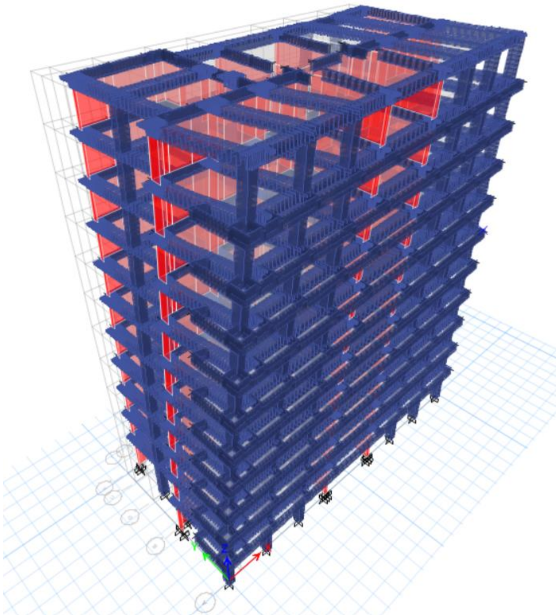

Fig. 5 - Mode 1 of Vibration T1=0.66 seconds (Translation in the Transverse Direction)

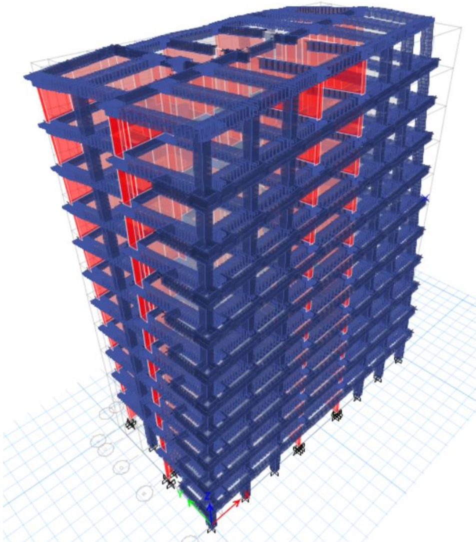

Fig. 6 - Mode 2 of Vibration T2=0.59 seconds (Torsion)

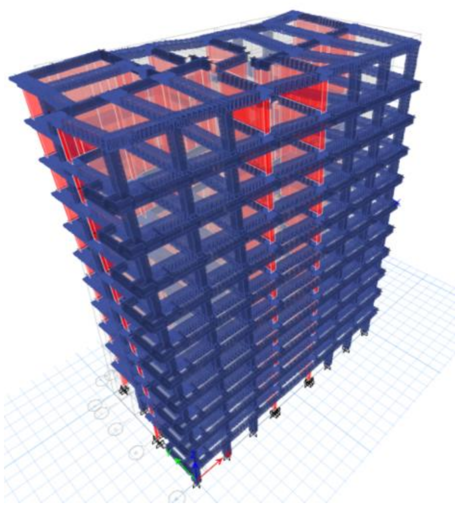

Fig. 7 - Mode 3 of Vibration T3=0.5 seconds (Translation in the Longitudinal Direction)

Table 1

Modal Participation Factors

Case	Mode	Period (sec)	UX	UY	SumUX	SumUY	RZ	SumRZ
Modal	1	0.656	1.14%	57.01%	1.14%	57.01%	13.60%	13.60%
Modal	2	0.586	2.79%	10.77%	3.93%	67.78%	58.13%	71.73%
Modal	3	0.491	66.18%	2.89%	70.11%	70.67%	1.23%	72.96%
Modal	4	0.168	0.08%	7.89%	70.19%	78.56%	8.45%	81.41%
Modal	5	0.138	0.22%	9.89%	70.41%	88.44%	7.99%	89.41%
Modal	6	0.111	19.91%	0.20%	90.32%	88.65%	0.11%	89.51%

Based on the modal analysis, as shown in *Table 1* above, the first mode of vibration is characterized by a transverse translation, involving 57% of the structure's mass. The second mode of vibration is represented by torsion, involving 58% of the structure's mass, while the third mode exhibits longitudinal translation, involving 67% of the structure's mass. This indicates that the structure is susceptible at torsion and was not well-conformed to the provisions of the P100-1/2013 [3] standard.

4. Nonlinear Static Analysis, PUSH-OVER

4.1. Nonlinearity Modeling

In the nonlinear analysis conducted using PERFORM 3D, two types of inelastic models were utilized [4] to capture the nonlinear behavior of structural elements:

Point Plastic Hinge Model with Interaction Surfaces – This approach defines discrete plastic hinges at specific locations (e.g., at the start and end of beams and columns) based on interaction surfaces that account for moment-axial force interaction. The moment-rotation behavior of these hinges was derived from FEMA 356 [5] provisions.

Fiber Model – The structural walls were discretized into multiple fibers, with each fiber assigned a specific stress-strain relationship for concrete and reinforcement steel. This model captures distributed inelasticity and provides a more refined representation of structural response under seismic loading.

The beams were defined using "INELASTIC FEMA BEAM, Concrete Type" elements [6]. For this type of finite element, the plastic hinges at the ends of the elements exhibit a rigid-plastic moment-rotation relationship. The moment-rotation relationship for each hinge is calculated by deriving the moment-rotation relationship for the corresponding component from the FEMA [5] standard and eliminating the elastic rotations.

The procedure is illustrated in the figure below (Fig. 8). It provides the relationship between the end moment and plastic rotation for the beam component according to the FEMA [5] standard, representing the moment-rotation relationship required for the hinge.

In the analysis, shear forces were neglected in the inelastic modeling. This assumption was justified by the fact that the structural walls have significant shear capacity due to their high reinforcement ratios and aspect ratios. Consequently, the failure mode is expected to be governed by flexural behavior rather than shear failure.

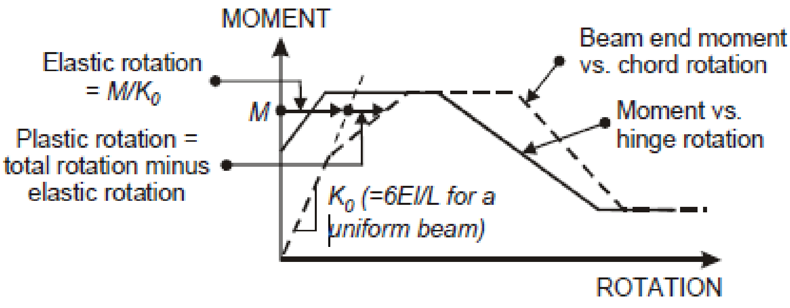

Fig. 8 - The Moment-Rotation relationship for the plastic hinge [6]

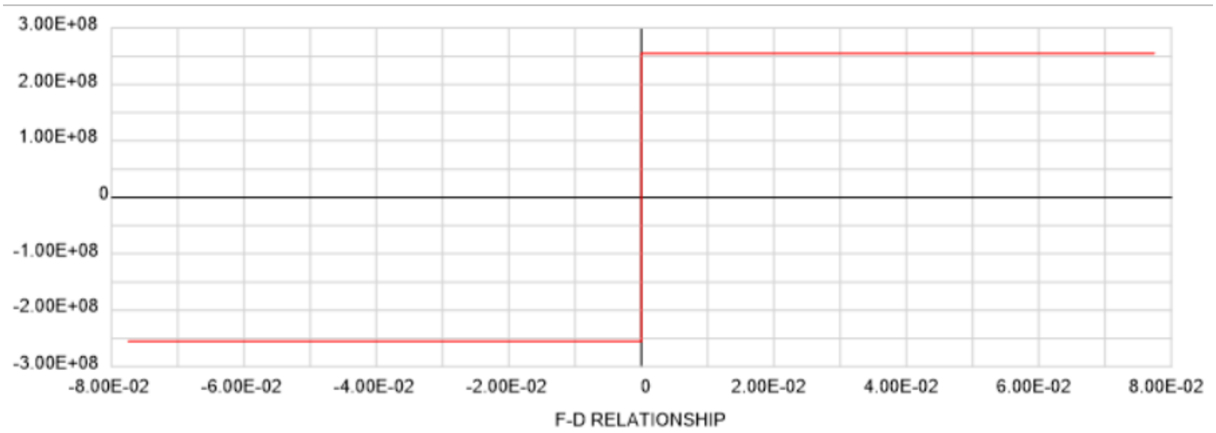

Fig. 9 - The behavior of discrete plastic hinges associated with beams: after reaching the specified moment capacities, the elements retain their strength regardless of the rotation values. (graph in N-mm)

The columns were defined using "INELASTIC FEMA COLUMN, Concrete Type" elements [6]. The steps for implementing concrete column components according to the FEMA standard are essentially the same as for a beam, but for columns, the axial force is considered. Thus, an interaction curve P-M and an interaction curve Mx-My are defined for these elements, as illustrated in the figure below (Fig. 10).

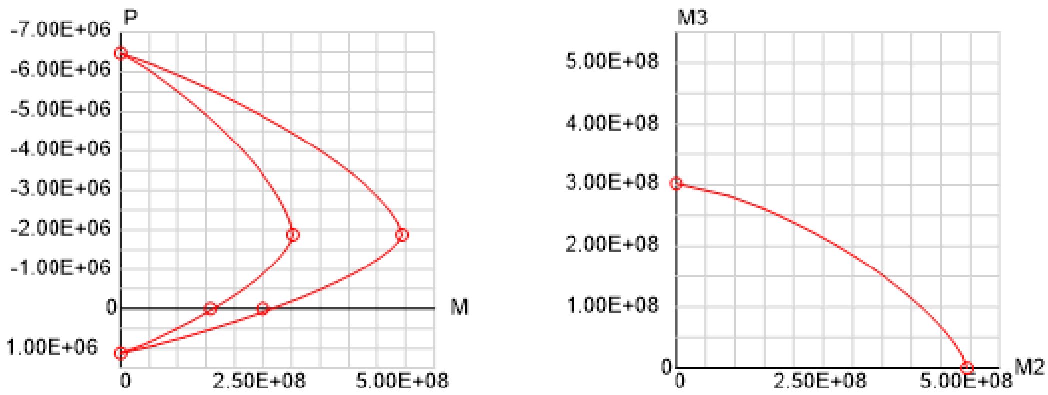

Fig. 10 - P-M and Mx-My Interaction Curves

The wall sections were discretized and divided into fibers, each associated with a specific σ-ε behavior law.

In the nonlinear analysis conducted in PERFORM 3D, the reinforcement steel (PC60) was modeled using an elastic-perfectly plastic (E-P-P) constitutive law, meaning it exhibits linear elastic behavior up to the yield stress, beyond which it maintains a constant stress level without strain hardening. For concrete, a trilinear stress-strain relationship was adopted, capturing the initial elastic response, a peak strength point, and a post-peak softening branch. The analysis did not consider confined concrete, meaning no additional strength or ductility enhancement from transverse reinforcement was included, leading to a more brittle post-peak response compared to confined models, which could influence the predicted seismic performance.

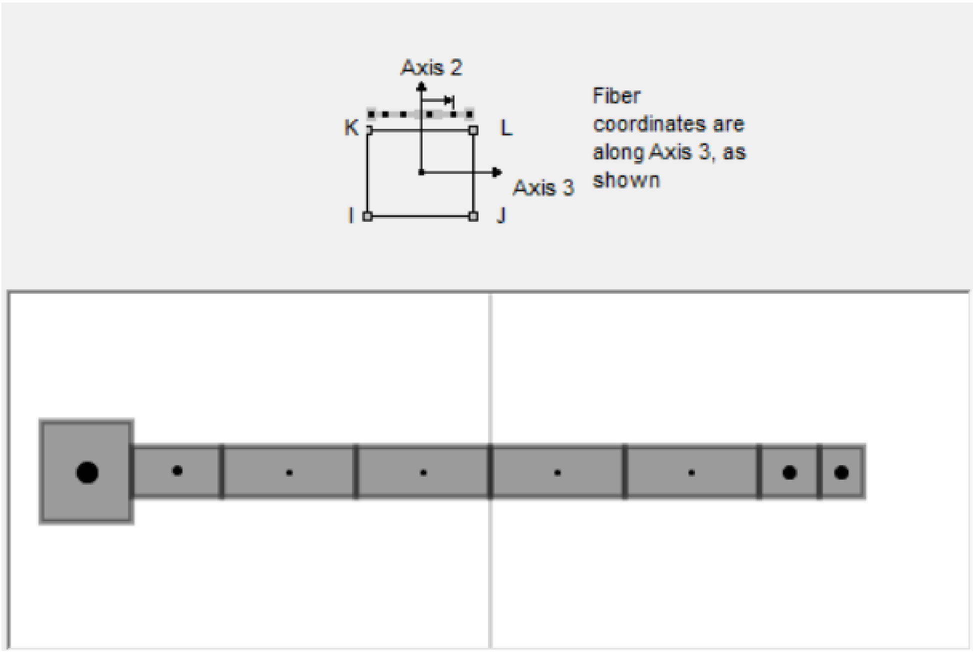

Fig. 11 - Concrete fibers and steel fibers defined in Perform3D

4.2. Determination of Capacity Curves

Through nonlinear static analysis approach, we assess the structure's base shear forces under extreme loading conditions by applying a monotonically increasing external load. It is important to note that while this method does not fully capture the true dynamic forces experienced in real-world scenarios, it effectively estimates the structure's capacity to withstand applied loads. Moreover, the analysis delineates the sequence in which structural elements begin to yield under constant stress. These findings are essential for understanding the behavior of the structure under maximum load conditions and for ensuring that any failure occurs in a controlled manner, thereby preventing brittle collapse and safeguarding both occupant safety and overall structural integrity.

The nonlinear static pushover analysis in PERFORM 3D was conducted using a force distribution proportional to modal displacements, applying monotonically increasing lateral loads based on a selected mode shape. The analysis followed the standard pushover procedure in PERFORM 3D, focusing on Mode 1 (translational in the transverse direction, Y-axis) and Mode 3 (translational in the longitudinal direction, X-axis) to evaluate the structural response in both principal directions. These pushover forces were applied at each floor level, mimicking the displacement patterns of the respective vibration modes. This approach allowed assessing the progression of plastic hinges and the global deformation capacity under increasing lateral loads.

Based on the capacity curves, displacement demands will be determined for events with average recurrence intervals of 40, 225, and 475 years. These intervals correspond to the limit states specified in the P100-3/2019 [7] design code, as follows:

- 40 years for the serviceability limit state,
- 225 years for the ultimate limit state,
- 475 years for the survival limit state.

The capacity curves derived from the nonlinear analysis illustrate the relationship between the base shear force and the displacement of a control point positioned at the top of the structure, capturing the structural response as loading progresses.

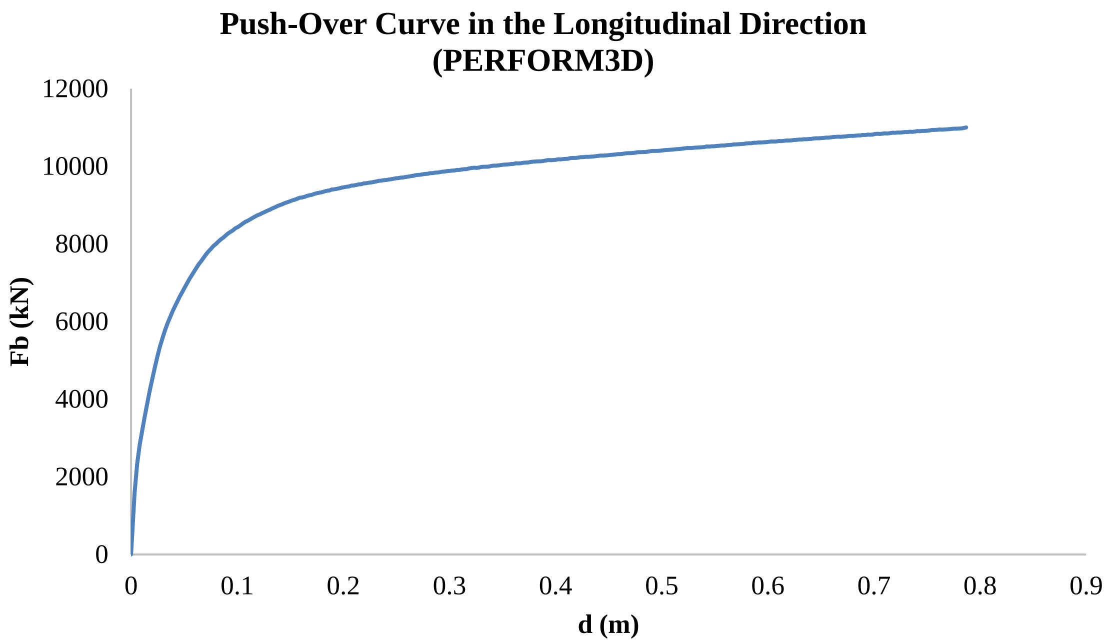

Fig. 12 - Push-Over Curve in the Longitudinal Direction

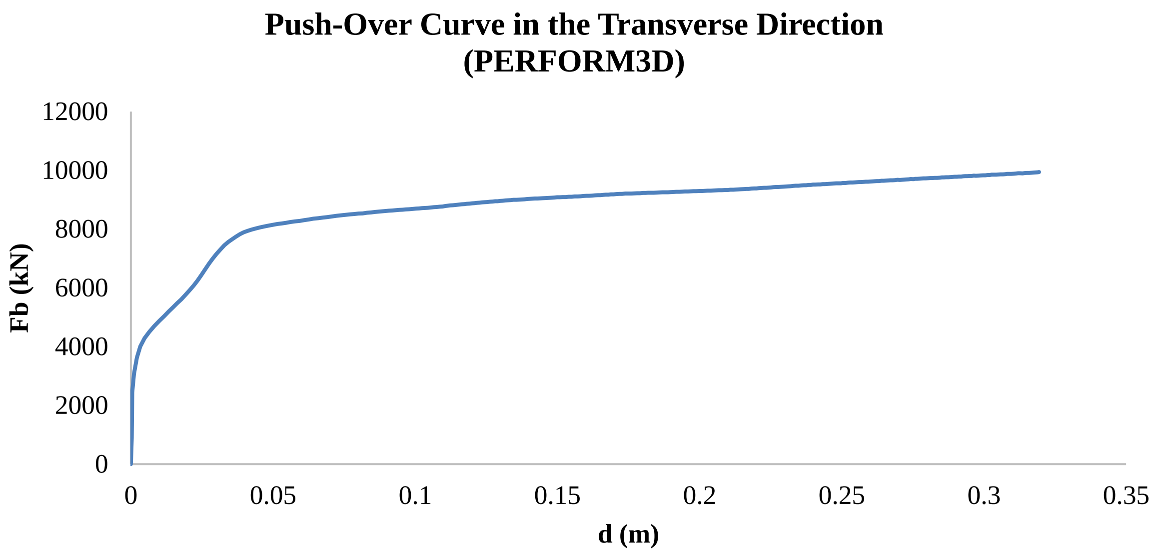

Fig. 13 - Push-Over Curve in the Transverse Direction

4.3. Determination of Displacement Demands

The displacement demands are approximated according to Annex B of SR EN 1998-1/2004 [8].

The required displacement is the value used to verify plastic rotations and lateral displacements. This displacement demand is determined for an equivalent single-degree-of-freedom (SDOF) system. A simplified analysis can be performed based on inelastic displacement spectra [9].

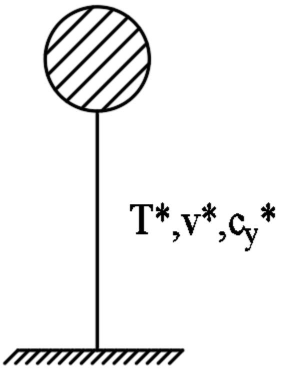

T^* - The natural period of the system

ν^* - Fraction of Critical Damping

$c_y{}^*$ - Normalized Yield Force

Fig. 14 - Single-Degree-of-Freedom (SDOF) System

Mass of the Equivalent System:

$$m^* = \sum_{i=1}^{n} m_i \Phi_i \text{ , where} \tag{1}$$

m_i -mass of a story,

Φ_i - normalized displacements for the mode shape of vibration ($\Phi_n = 1.0$).

Transformation Factor:

$$\Gamma = \frac{m^*}{\sum_{i=1}^{n} m_i \cdot \Phi_i^2} \tag{2}$$

The Force F* and Displacement d* of the SDOF System:

$$F^* = \frac{F_b}{\Gamma} \tag{3}$$

$$d^* = \frac{d_n}{\Gamma} \tag{4}$$

F_b - Base Shear Force of the MDOF System,

d_n - Control Node Displacement.

Determination of the Bilinearized Curve According to CR2-1-1.1/2022 [10].

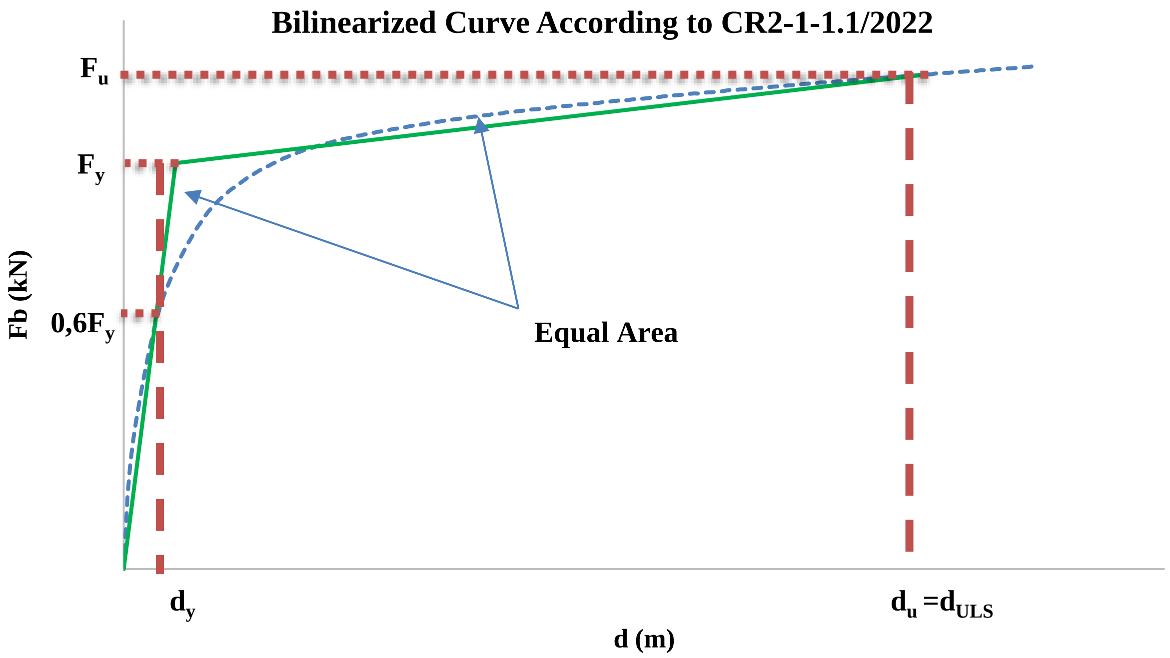

Fig. 15 - Schematic Representation of the Horizontal Force–Horizontal Displacement Response Law

To bilinearize the response law, the quasi-elastic response segment was extended until it intersected with the response law determined through nonlinear static analysis at a horizontal force value equal to 60% of the conventional yield force, F_y [10].

The values of the yield force F_y and the yield displacement d_y were determined such that the elasto-plastic deformation energy corresponding to the bilinear response law is equal to that of the response law obtained through nonlinear static analysis [10].

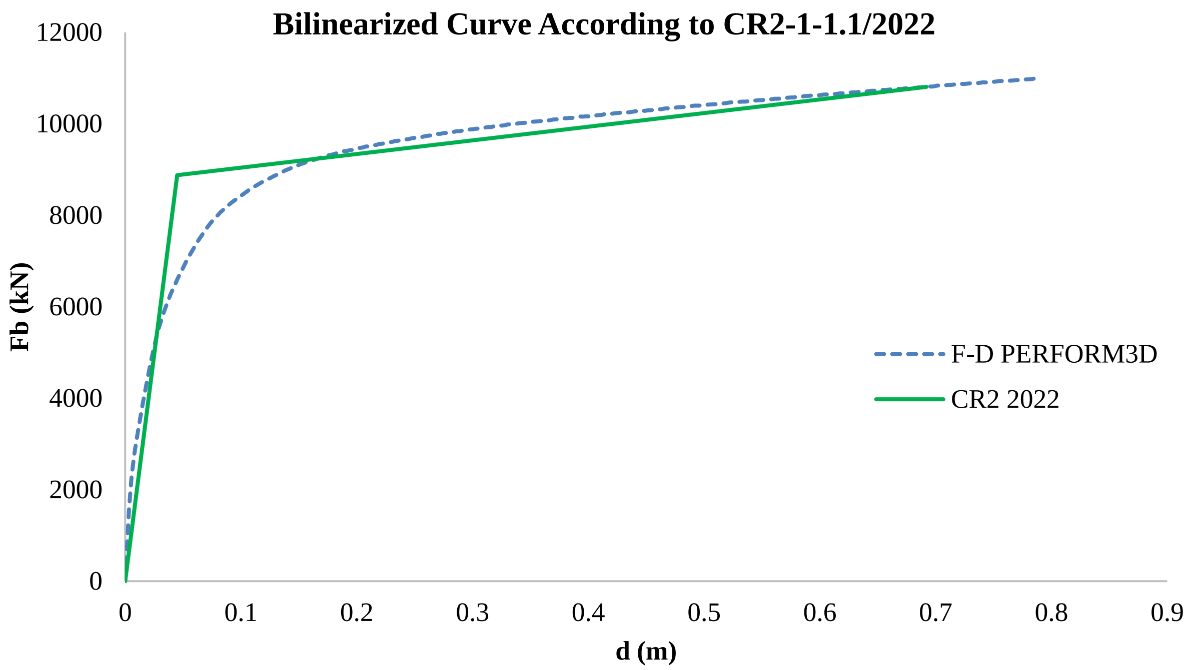

Fig. 16 - Bilinearization of the Horizontal Force–Horizontal Displacement Curve in the Longitudinal Direction

Determination of the Natural Period of the Equivalent SDOF System

$$T^* = 2\pi\sqrt{\frac{m^* \cdot d_y^*}{F_y^*}} \tag{5}$$

To determine the displacement demand for an equivalent single-degree-of-freedom (SDOF) system, the capacity spectrum method was applied using modified N2 inelastic spectra, as detailed in Fajfar's article [11]. These spectra were adjusted using behavior factors as proposed by Miranda et al. [12], incorporating the effects of earthquake characteristics and local site conditions. The material's hysteretic behavior was modeled as bilinear, aligning with standard practices in seismic performance evaluation.

Once the displacement demand was determined using the modified N2 inelastic spectra, a set of three artificial accelerograms was generated with SeismoArtif [13] to match the target spectrum. These accelerograms were designed to be compatible with the design spectrum and were used to generate inelastic spectra that accurately reflect the system's inelastic response characteristics.

We used the elastic spectrum defined in P100-1/2013 modified in 2019 [3] as a baseline. Thus, the horizontal force–horizontal displacement graph for a single-degree-of-freedom (SDOF) system was intersected with the inelastic spectrum proposed by Miranda [12] , along with three additional inelastic spectra generated using the PRISM software [14]. These intersections collectively define the displacement demand for the SDOF system, ensuring a detailed assessment of its seismic response under varying conditions.

The behavior factors proposed by Miranda are:

$$q_0 = \frac{\mu - 1}{\Phi} + 1 \geq 1 \quad (6)$$

where,

q_0 - reduction factor for inelastic demand

μ - ductility factor

Φ - site and seismic characteristics adjustment

$$\Phi = 1 + \frac{T_c}{3T} - \frac{3T_c}{4T} e^{\left[-3\left(ln\left(\frac{T}{T_c}\right) - \frac{1}{4}\right)^2\right]} \quad (7)$$

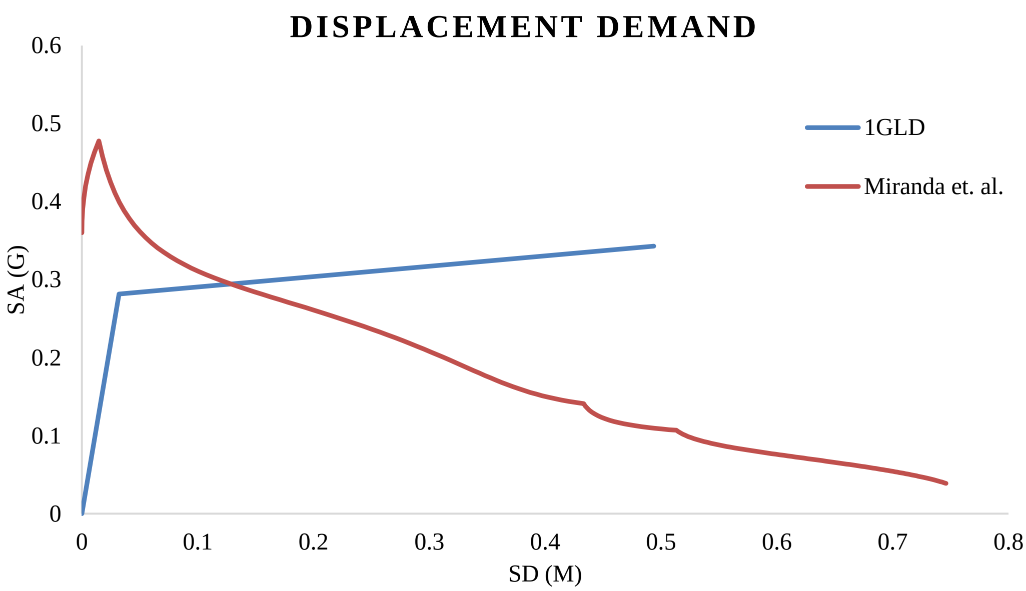

Fig. 17 - The intersection of the bilinearized Push-Over curve for an SDOF system with the inelastic spectrum proposed by Miranda.

To transform the displacement demand from a single-degree-of-freedom (SDOF) system to a multi-degree-of-freedom (MDOF) system, the following relationship is used:

$$d_t = \Gamma \cdot d_t^* \qquad (8)$$

Table 2

Determination of the displacement demand in the longitudinal direction for an MDOF system

MRP (years)	Associated Limit State	Displacement Demand Miranda et. al. (m)	Displacement Demand inelastic spectra 1 (m)	Displacement Demand inelastic spectra 2 (m)	Displacement Demand inelastic spectra 3 (m)
40	SLS	0.079	0.065	0.064	0.058
225	ULS	0.217	0.203	0.192	0.197
475	CP	0.28	0.249	0.304	0.337

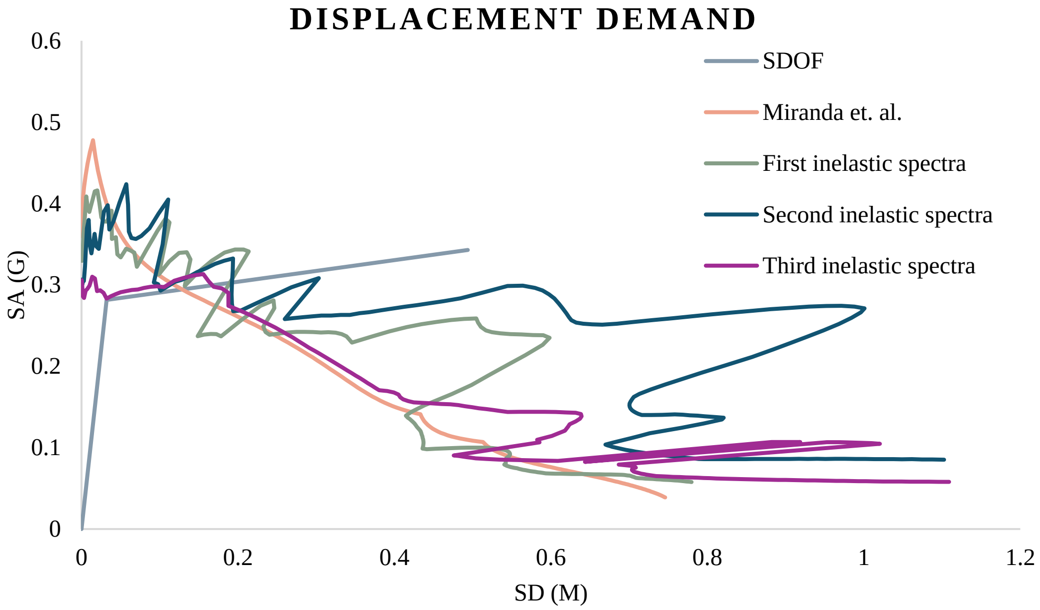

Fig. 18 - Displacement demands for various inelastic spectra in the longitudinal direction

Table 3

Determination of the displacement demand in the transverse direction for an MDOF system

MRP (years)	Associated Limit State	Displacement Demand Miranda et. al. (m)	Displacement Demand inelastic spectra 1 (m)	Displacement Demand inelastic spectra 2 (m)	Displacement Demand inelastic spectra 3 (m)
40	SLS	0.031	0.024	0.021	0.023
225	ULS	0.095	0.097	0.11	0.087
475	CP	0.125	0.188	0.121	0.176

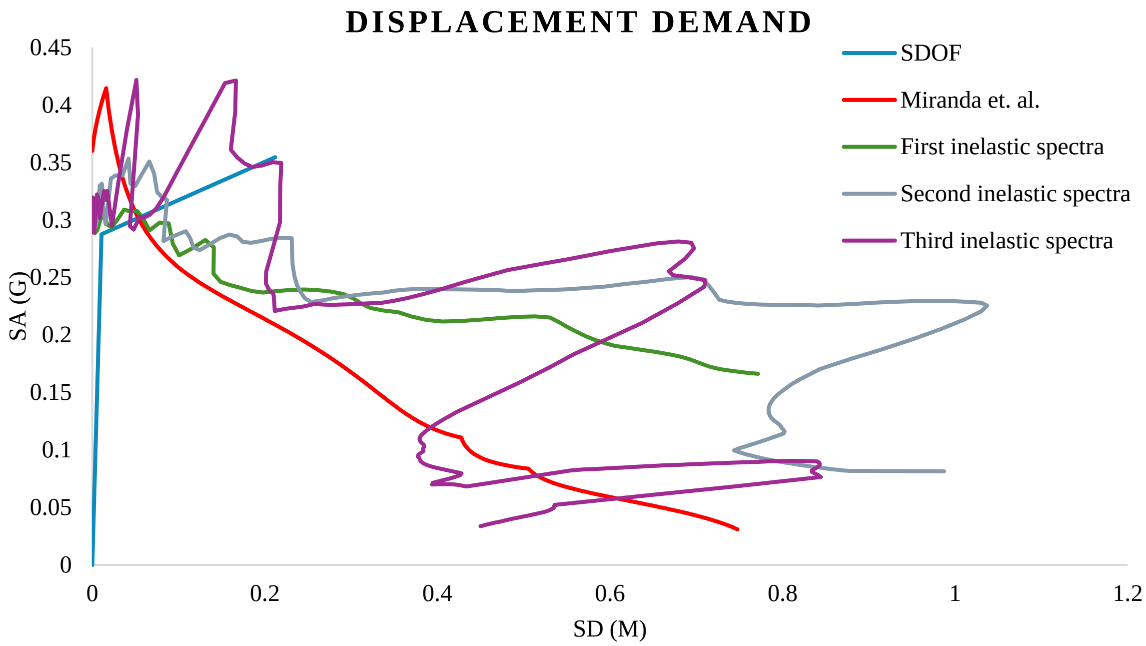

Fig. 19 - Displacement demands for various inelastic spectra in the transverse direction

From

Fig. 18 and Fig. 19, it is evident that using the P100-1/2013 (modified 2019) elastic spectrum as a baseline, then intersecting the SDOF curve with Miranda's inelastic spectrum and the three additional inelastic spectra (generated via PRISM) yields a range of displacement demands in the longitudinal direction. These variations highlight how different inelastic modeling assumptions (e.g., ductility, hysteretic behavior) can significantly influence predicted seismic response. By examining multiple inelastic spectra rather than relying on a single code-based curve, the analysis provides a more comprehensive view of the SDOF system's behavior under various seismic intensity levels. This multi-spectrum approach allows to capture a broader set of possible responses, thereby enhancing confidence in the displacement-based design and the overall seismic assessment.

4.4. Plastic Mechanism Based on the Associated Limit State

The plastic mechanism represents the sequence and distribution of plastic hinges that form in the structure as it reaches different limit states. The development of plastic hinges is directly influenced by the structure's capacity to dissipate energy through inelastic deformations, ensuring the building's stability during seismic events.

Further, I will use the adjusted mean values of the displacement demands to determine the structure's performance under different limit states.

The adjusted mean is a modified average value that accounts for the variability in displacement demand. It is calculated by applying a correction factor to the mean displacement value based on the normalized sum of squared deviations and a statistical adjustment factor (1.645 for a 5% probability of exceedance).

Assuming a normal distribution of the ground motion values, ASCE/SEI 7-22 [15] recommends using a minimum of seven records for nonlinear time-history analyses. The normality assumption further justifies the use of standard statistical parameters (e.g., the 1.645 factor for 5% exceedance in a one-tailed test) when quantifying the seismic response variability.

Mean Displacement:

$$d_{mean} = \frac{\sum d}{n} \tag{9}$$

d - individual displacement values.

n - total number of displacement values

Squared Deviations from the Mean

$$(d - d_{mean})^2 \tag{10}$$

Sum the Squared Deviations

$$\sum (d - d_{mean})^2 \tag{11}$$

Normalized Sum

$$Normalized\ Sum = \frac{\sum (d - d_{mean})^2}{d_{mean}} \tag{12}$$

Adjustment Factor

$$d_{adjusted} = d_{mean} \cdot (1 - 1.645 \cdot Normalized\ Sum) \tag{13}$$

1.645 is the z-value for a 95% confidence level in a one-tailed normal distribution

Table 4

Adjusted mean displacement demand on longitudinal direction for various limit states

Associated Limit State	d (m)	d_{mean} (m)	$(d-d_{mean})^2$	$\sum(d-d_{mean})^2$	Normalized Sum	Adjusted Mean (m)
SLS	0.079	0.0665	0.00015625	0.00005925	0.000891	0.066
	0.065		0.00000225			
	0.064		0.00000625			
	0.058		0.00007225			
ULS	0.217	0.2023	0.00021756	8.7688E-05	0.0004336	0.202
	0.203		0.00000056			
	0.192		0.00010506			
	0.197		0.00002756			
CP	0.28	0.2925	0.00015625	0.00104025	0.0035564	0.291
	0.249		0.00189225			
	0.304		0.00013225			
	0.337		0.00198025			

Table 5

Adjusted mean displacement demand on transverse direction for various limit states

Associated Limit State	d (m)	d_{mean} (m)	$(d-d_{mean})^2$	$(d-d_{mean})^2$	Normalized Sum	Adjusted Mean (m)
SLS	0.031	0.0248	0.00003906	1.4188E-05	0.0005732	0.025
	0.024		0.00000056			
	0.021		0.00001406			
	0.023		0.00000306			
ULS	0.095	0.0973	0.00000506	6.8188E-05	0.0007012	0.097
	0.097		0.00000006			
	0.11		0.00016256			
	0.087		0.00010506			

Associated Limit State	d (m)	d_{mean} (m)	$(d-d_{mean})^2$	$(d-d_{mean})^2$	Normalized Sum	Adjusted Mean (m)
CP	0.125	0.1525	0.00075625	0.00089025	0.0058377	0.151
	0.188		0.00126025			
	0.121		0.00099225			
	0.176		0.00055225			

4.4.1. Deformed shape on longitudinal direction

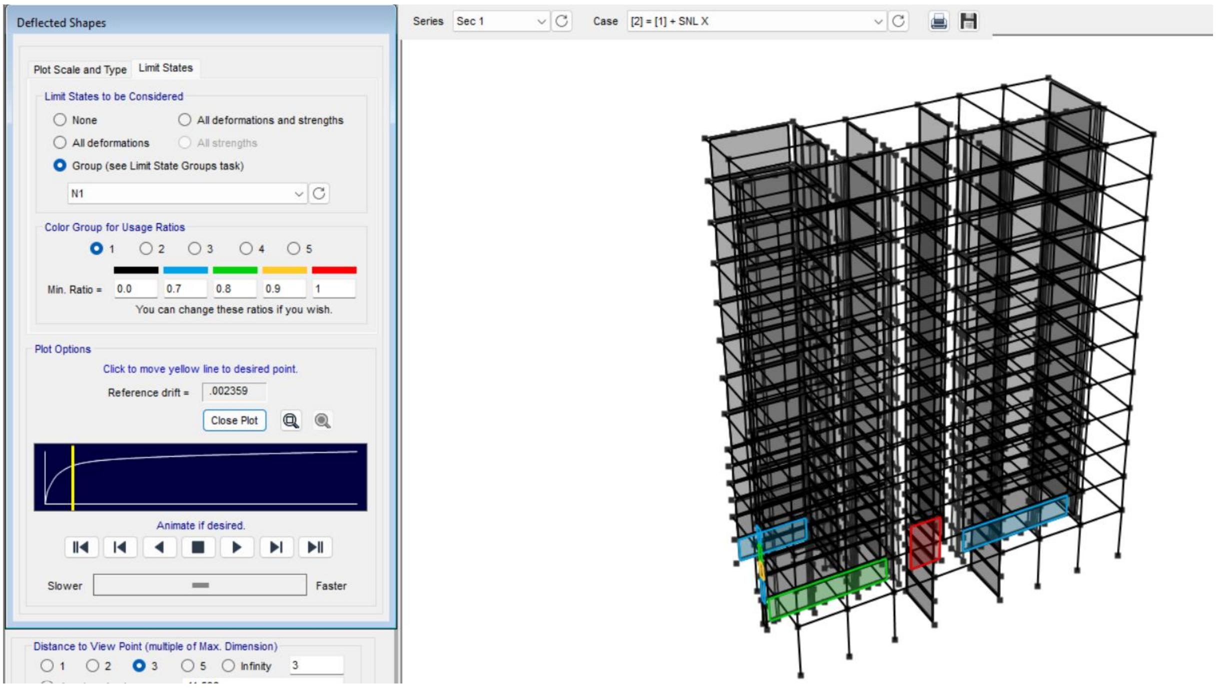

Fig. 20 - The plastic hinges mechanism of elements corresponding to a displacement of 0.066 m associated with a 40-year return period earthquake

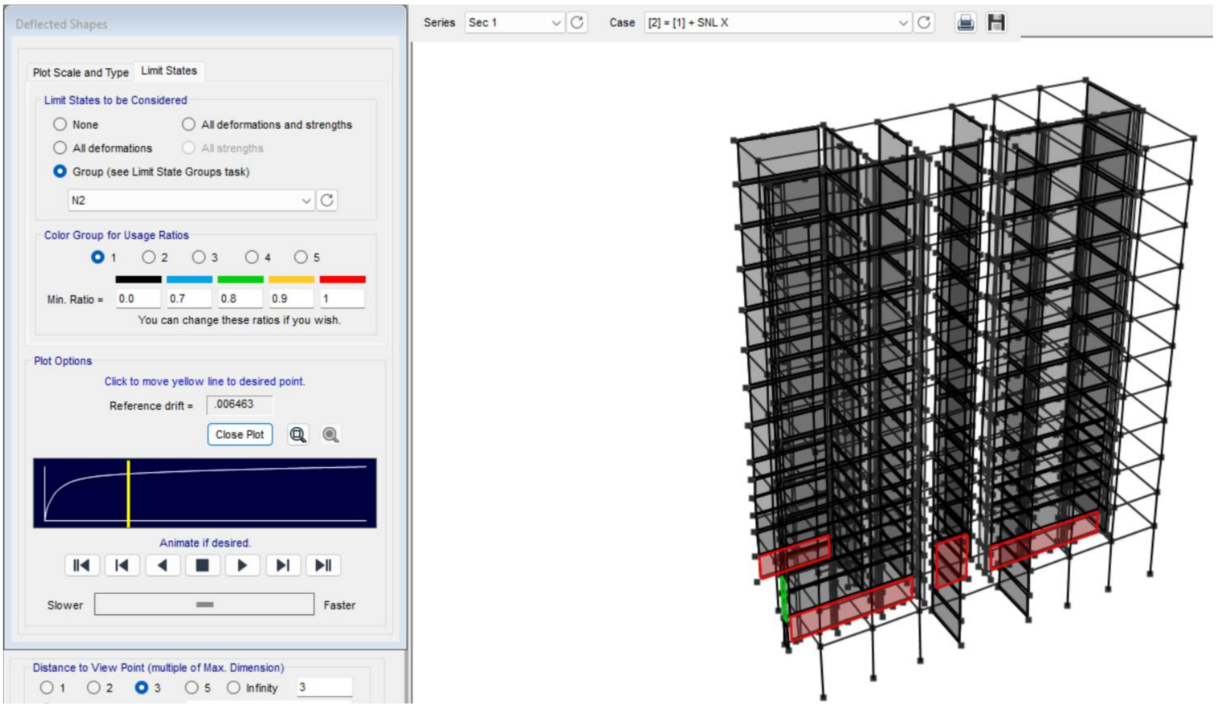

Fig. 21 - The plastic hinges mechanism of elements corresponding to a displacement of 0.202 m associated with a 225-year return period earthquake

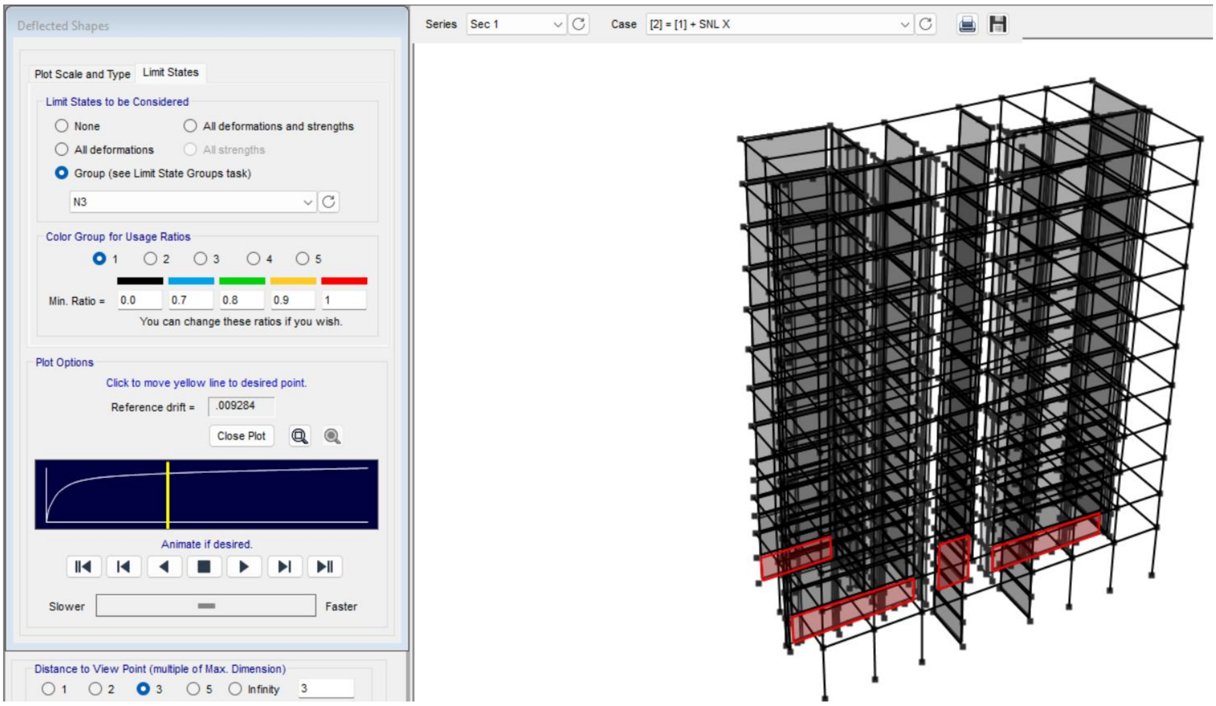

Fig. 22 - The plastic hinges mechanism of elements corresponding to a displacement of 0.291 m associated with a 475-year return period earthquake

The plastic hinge mechanisms shown in the figures above indicate the progressive failure of the structure under increasing seismic displacement demands, corresponding to earthquakes with different Mean Return Intervals (MRI). The formation of plastic hinges is concentrated at the base of the longitudinal walls, where critical deformation is observed. These rotation capacities were determined using Table 6-18 from FEMA 356 [5].

For an earthquake with a 40-year MRI (Fig. 20), the plastic hinges are formed in the longitudinal walls, reaching their rotation capacity at a displacement of 0.066 m, corresponding to the Immediate Occupancy limit state.

In the case of a 225-year MRI earthquake (Fig. 21), the plastic hinges extend further, and the rotation capacity at the base of the walls is exceeded at a displacement of 0.202 m, indicating the Collapse Prevention limit state.

For a 475-year MRI earthquake (

Fig. 22), the plastic mechanism fully develops, with widespread plastic hinges in the longitudinal walls at a displacement of 0.291 m, corresponding to the Survival Limit State.

These results emphasize that the failure mechanism initiates at critical wall sections, primarily due to exceeding the rotation capacity in plastic zones.

4.4.2. Deformed shape on transverse direction

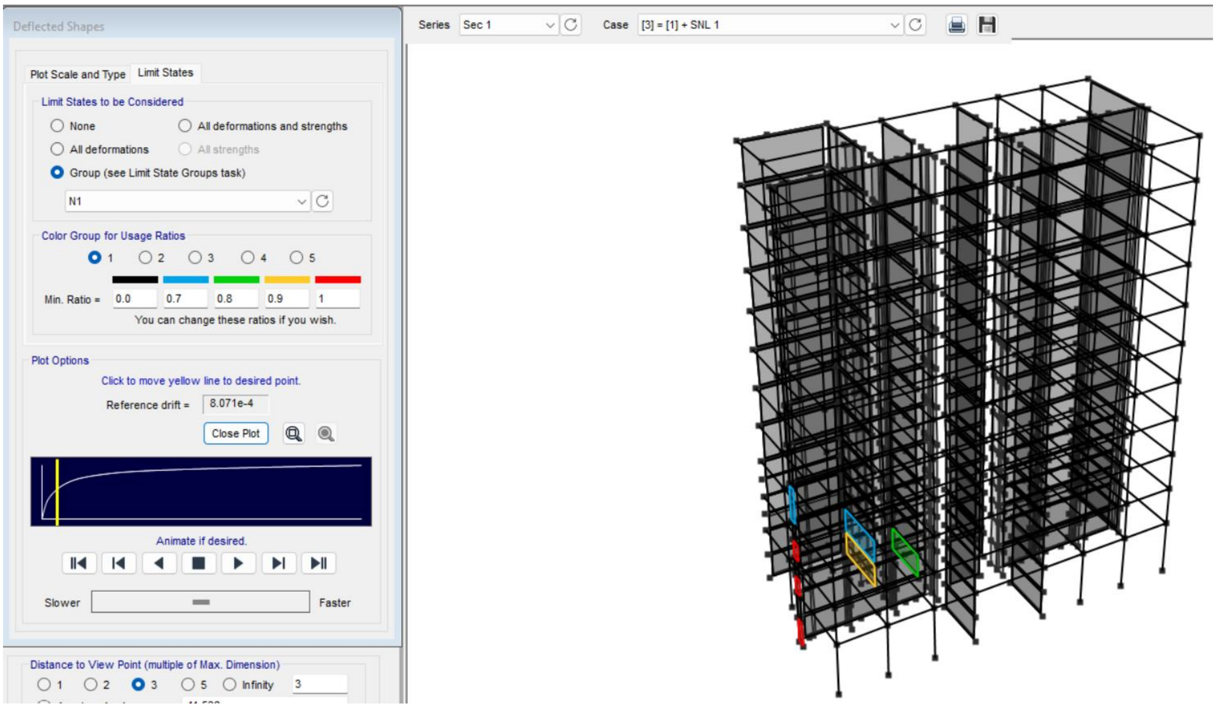

Fig. 23 - The plastic hinges mechanism of elements corresponding to a displacement of 0.025 m associated with a 40-year return period earthquake

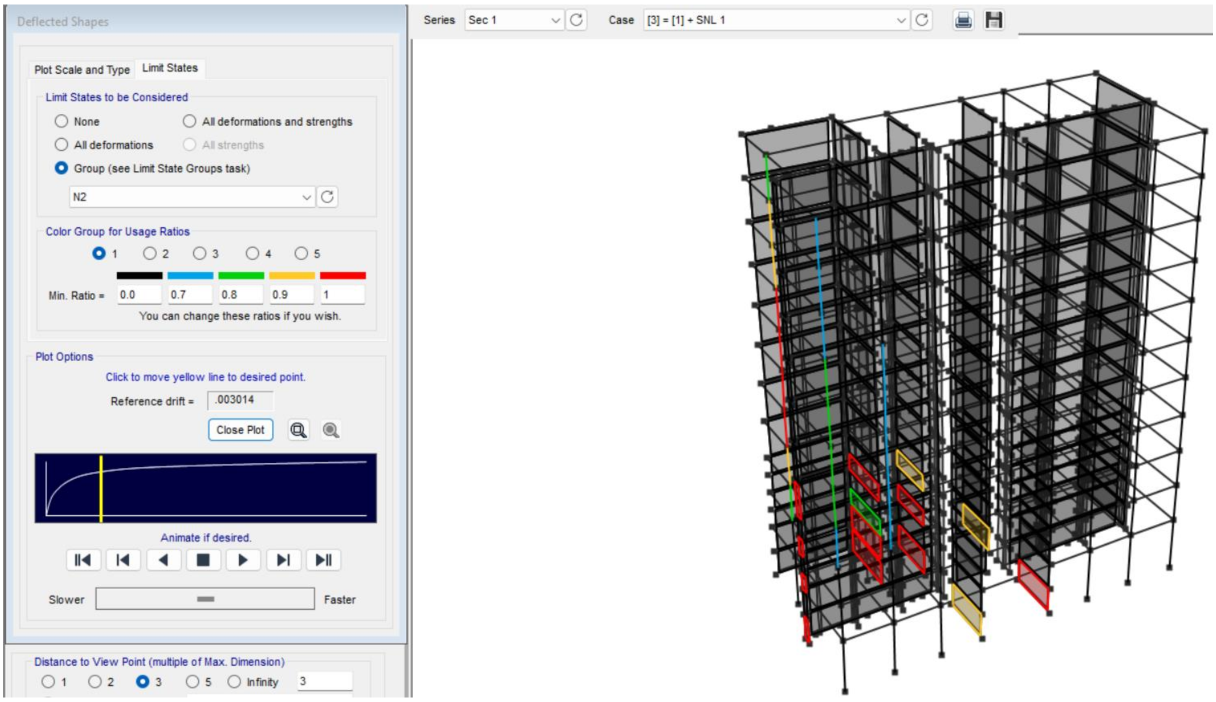

Fig. 24 - The plastic hinges mechanism of elements corresponding to a displacement of 0.202 m associated with a 225-year return period earthquake

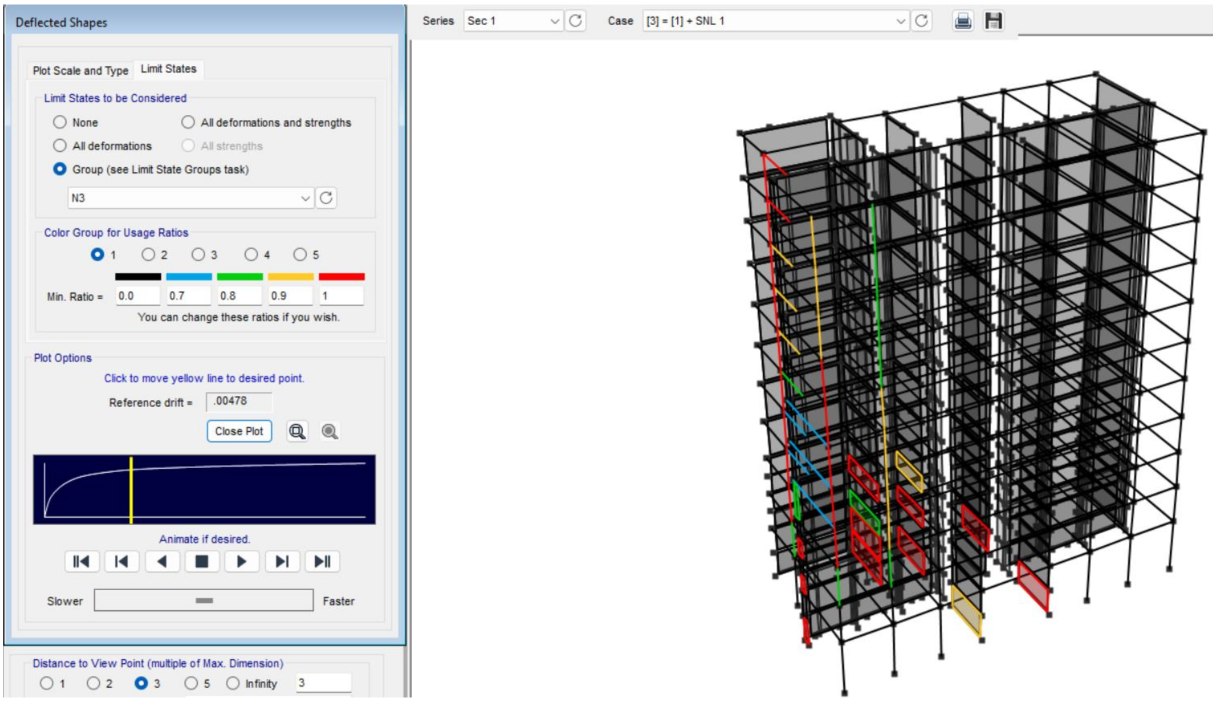

Fig. 25 - The plastic hinges mechanism of elements corresponding to a displacement of 0.151 m associated with a 475-year return period earthquake

The plastic hinges mechanism illustrated in figures above reveals the progressive development of plastic hinges in both the walls and columns, particularly in critical zones, due to increasing displacement demands associated with different seismic return periods. The failure mechanism is governed by both flexural behavior and global torsional effects at the structural level, resulting in the exceedance of the rotation capacities in key structural elements. These rotation capacities were determined using Table 6-18 from FEMA 356 [5].

For a 40-year MRI earthquake (Fig. 23), the plastic mechanism is observed at a peak displacement of 0.025 m, mainly affecting the transverse walls and some columns, corresponding to the Immediate Occupancy limit state.

In the case of a 225-year MRI earthquake (Fig. 24), a more pronounced plastic mechanism develops, with multiple transverse walls and columns exceeding their rotation capacity at a displacement of 0.202 m, corresponding to the Collapse Prevention limit state.

For a 475-year MRI earthquake (

Fig. 25), widespread plastic hinges are observed in the transverse walls, columns, and beams at a displacement of 0.151 m, corresponding to the Survival Limit State.

The figures highlight that structural failure initiates in the critical wall sections due to torsional effects, necessitating retrofitting measures to improve seismic resilience and prevent failure during significant seismic events.

4.4.3. Evaluation of Deformation Capacity in the Critical Zones of Walls

To evaluate the deformation capacity in the critical zones, two characteristic walls of the structure were selected: one in the longitudinal direction (P1X) and one in the transverse direction (P1Y). The calculation was performed based on the formulas provided in CR2-1-1.1/2013 [16], based on formulas provided by Paulay [17] .

The rotation capacity in the conventional plastic hinge is obtained using the following equation:

$$\theta_{pl,u} = \frac{1}{\gamma_{el}} \cdot (\phi_u - \phi_y) \cdot L_{pl} \tag{14}$$

where:

ϕ_u - ultimate curvature

ϕ_y - curvature at the initiation of yielding in the tension reinforcement

L_{pl} - conventional length of the plastic zone

$\gamma_{el} = 1.5$ - safety factor

The ultimate curvature ϕ_u and ϕ_y values were determined using the general calculation method for reinforced concrete elements under bending [18], no additional concrete confinement was considered in the bulb regions end zones. This method relies on the equilibrium conditions of the cross-sections, the geometric assumptions of the plane sections theory, and the material behavior laws for concrete and steel.

The elastic component of the rotations is determined using the following equation:

$$\theta_y = \frac{1}{3} \cdot \phi_y \cdot L_v \tag{15}$$

where:

$$L_v = \frac{M}{V}\text{, shear lever arm} \tag{16}$$

To determine the length of the plastic zone, the following equation is used:

$$L_{pl} = 0.1 \cdot L_V + 0.15 \cdot h_w + 0.25 \cdot \frac{d_{bL} \cdot f_{yk}}{\sqrt{f_{ck}}} \tag{17}$$

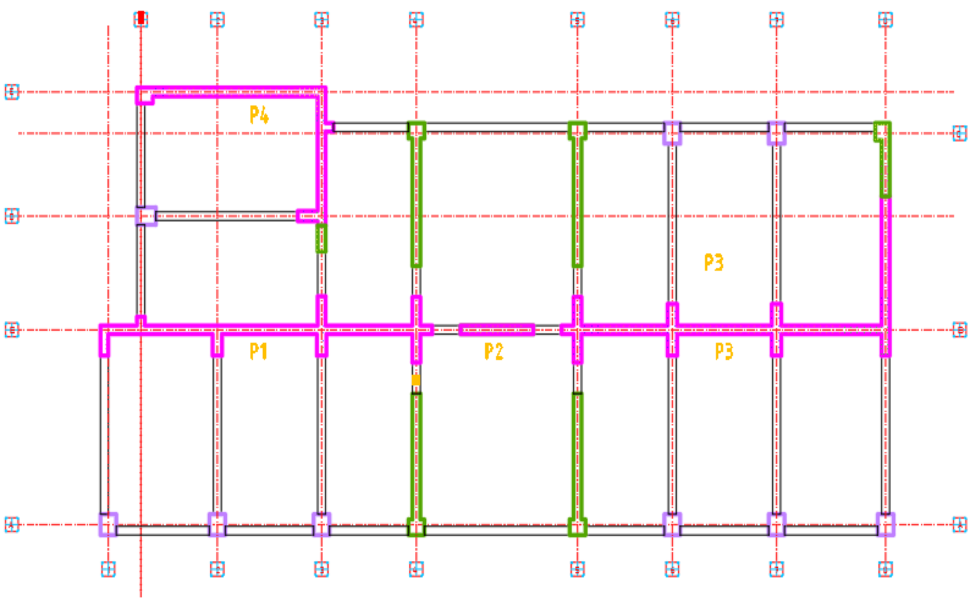

Fig. 26 - Layout of walls in the longitudinal direction (X)

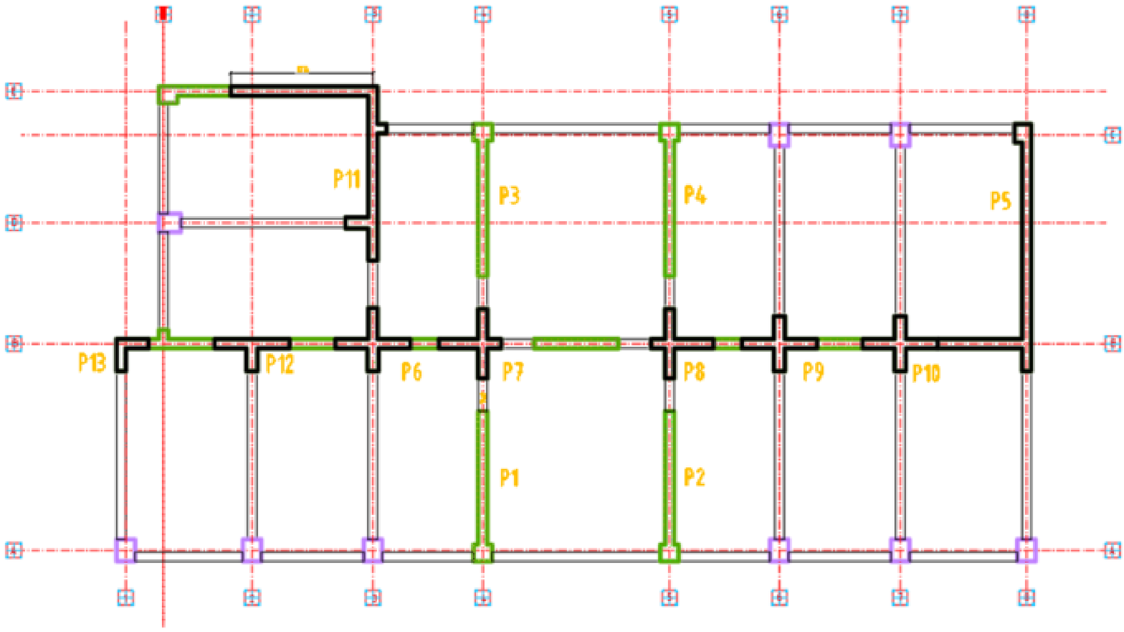

Fig. 27 - Layout of walls in the transverse direction (Y)

Table 6

Determination of the Walls' Rotation Capacity

Wall	hw (m)	ϕ_y (rad/m)	ϕ_{ul} (rad/m)	Lv (m)	Lpl (m)	θ_y (rad)	γ_{el}	$\theta_{pl,u}$ (rad)	θ_u^{ULS} (rad)	$\theta_u^{Perform3d}$ (rad)	Exceedance
P1x	31.47	0.00028	0.003124	17.07	6.918	0.00157	1.5	0.0131	0.0147	0.022	1.52
P1y	31.47	0.00071	0.008775	10.75	6.286	0.00253	1.5	0.0338	0.0363	0.057	1.58

Both walls, P1X and P1Y, exceed their rotation capacities, indicating that the structure is vulnerable to plastic deformations beyond its design limits under seismic loading. Even though the capable rotations can be considered identical for both walls, wall P1Y exhibits a slightly higher exceedance factor (1.58) compared to P1X (1.52). These results emphasize the need for reinforcement or retrofitting measures to ensure that the walls can sustain seismic loads without collapsing, with special attention required for wall P1Y due to its greater vulnerability.

5. Conclusions

The nonlinear analysis performed on the 10-story RC shear wall structure highlights the building's response to seismic loads across different limit states, corresponding to return periods of 40, 225, and 475 years. The study reveals that both longitudinal and transverse walls exceed their rotation capacities, indicating vulnerability to plastic deformations during seismic events. Wall P1Y shows a higher exceedance factor, making it more prone to failure compared to P1X. This demonstrates the necessity of retrofitting measures to improve the structure's performance, particularly in critical zones prone to failure.

The evaluation of displacement demands using the N2 method, as introduced by Fajfar et al. [11], provides a refined framework for assessing seismic response by integrating nonlinear structural characteristics. This approach, also known as the Capacity Spectrum Method, builds upon earlier developments dating back to Freeman in the 1970s [19]. The identification of plastic mechanisms through analysis reveals that structural failure initiates at critical points, underscoring the necessity of meticulous detailing and reinforcement strategies. The study further highlights the imperative of updating seismic codes to ensure that older buildings, originally designed under outdated standards, undergo adequate retrofitting to align with contemporary safety requirements.

Overall, the findings underscore the imperative of advancing design methodologies and retrofitting strategies to optimize the ductility and energy dissipation capacity of reinforced concrete structures. By enhancing these critical parameters, seismic resilience can be significantly improved, mitigating risks and preventing catastrophic structural failures.

Future work should focus on incorporating advanced computational models to simulate various seismic scenarios more accurately and evaluate the efficiency of different retrofitting strategies. Additionally, research could explore the use of new materials with higher ductility and energy dissipation capacity to improve the seismic performance of RC structures. Continuous monitoring and updating of seismic codes, based on recent earthquake data, will be essential to ensure the safety and resilience of buildings in seismic-prone areas.

Appendices

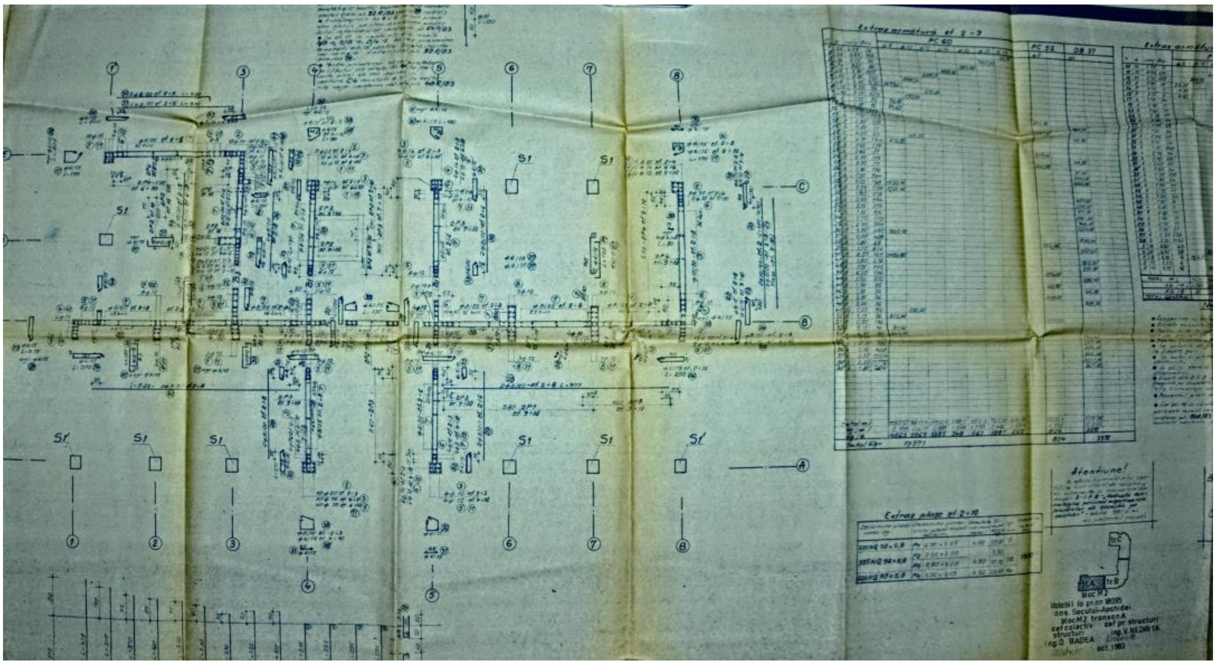

Fig. 28 - Wall Reinforcement Plan

References

[1] P100-81. (1982). Proiectarea antiseismica a construcțiilor de locuințe, social-culturale, agrozootehnice și industriale.

[2] EN 1992-1-1. 2004. Eurocode 2: Design of concrete structures - Part 1-1: General rules and rules for buildings.

[3] P100-1/2013. 2019. Cod de proiectare seismică-partea i prevederi de proiectare pentru clădiri.

[4] X. Chen, X. Han, F. Luo, S. Wu. 2011. Fiber element based elastic-plastic analysis procedure and engineering application, in: *Procedia Eng.* pp. 1807–1815. https://doi.org/10.1016/j.proeng.2011.07.227.

[5] Federal emergency management agency, federal emergency management agency fema 356, 2000.

[6] S. Inc. 2021. Components and Elements for Perform 3D. http://www.csiamerica.com/.

[7] P 100-3/2019 Cod de proiectare seismică-partea a III-a-prevederi pentru evaluarea seismică.

[8] SR EN 1998-1: 2004. Eurocod 8: Proiectarea structurilor pentru rezistenta la cutremur.

[9] Anil K. Chopra, Rakesh K. Goel. (1999). Capacity Demand Diagrams Based On Inelastic Response Spectra, *Earthquake Spectra 15*.

[10] CR 2-1-1.1/2022-Cod de proiectare a construcțiilor cu pereți structurali de beton armat.

[11] P. Fajifar, Capacity Spectrum Method Based On Inelastic Demand Spectra, *Earthq Eng Struct Dyn* (1999) 979–993.

[12] Eduardo Miranda, Vitelmo V Bertero. (1994). Evaluation of Strength Reduction Factors for Earthquake-Resistant Design, *Earthquake Spectra* 357–379. https://doi.org/https://doi.org/10.1193/1.1585778.

[13] Seismosoft Ltd. (2023). SEISMOAPPS-Technical-Information-Sheet-ENG.

[14] Seong-Hoon Jeong, Kwang-Ho Lee, Won-Seok Jang. (2025). PRISM for Earthquake Engineering A Program for seismic response analysis of SDOF systems User Manual, https://sem.inha.ac.kr/program/index.htm (accessed January 2, 2025).
[15] Minimum Design Loads and Associated Criteria for Buildings and Other Structures. 2021. *American Society of Civil Engineers*, Reston, VA. https://doi.org/10.1061/9780784415788.
[16] CR 2-1-1.1/2013. Cod de proiectare a construcciilor cu pereti structurali de beton armat.
[17] T. Paulay, M.J.N. Priestly. 1992. Principles of Member Design, in: *Seismic Design of Reinforced Concrete and Masonry Buildings*, Wiley. pp. 95–157. https://doi.org/10.1002/9780470172841.ch3.
[18] C.S. Whitneyt. (1937). Design of Reinforced Concrete Members Under Flexure or Combined Flexure and Direct Compression*, *Proceedings of the american concrete institute* 33 483–498. https://doi.org/https://doi.org/10.14359/8429.
[19] S.A. Freeman. (1978). Prediction of Response of Concrete Buildings to Severe Earthquake Motion, *ACI Symposium Publication 55*. https://doi.org/10.14359/6629.